Report Mumetal analysis

Marc Solar

July 11, 2019

Abstract

A cube with sides consisting of 1.25 mm thick sheets of mumetal and side length of approximately one meter, is degaussed and examined for its capacity to shield external magnetic fields of different frequencies and in three spatial axes. Particular focus is devoted to the vertical z axis, where shielding factors of up to 175 are found for low frequency external fields at the center of the cube. The analysis is repeated after removal of two opposing sides of the mumetal cube.

Contents

1 Introduction

Many applications, in particular in high precision fundamental physics require stable and well-known magnetic field environments. This is true in particular for searches for the neutron electric dipole moment (EDM) like the beam EDM experiment [1] [2] or the nEDM experiment. These searches usually employ spin-precession Ramsey techniques [3] entailing a precise interaction with magnetic fields. Time stability and homogeneity of the magnetic fields are therefore essential for these experiments due the coupling thereof with the spin of particles. Particularly, along the axis of quantization of along which the Larmor precession takes place in such experiments, the homogeneity of the field plays a major role in the final sensitivity of the measurement.

Passive magnetic shielding is employed to ensure low magnetic field background and low gradients thereof. The passive shielding consists of enclosed structures of mumetal. The high magnetic permeability of this material allows for a high magnetic flux therein, essentially leading the magnetic flux to pass around the enclosure instead of penetrating it. Mumetal shielding additionally increases field homogeneity as the shielding factor increases with the degree of the multipole [4].

A cubical enclosure of mumetal is characterized in terms of its shielding factor in all three axes. The mumetal layers are of 1.25 mm thickness and the cube sides measure roughly 1 m. Additional pieces of mumetal shielding are placed along the cube edges and in contact with the sides to guarantee full enclosure of the inside.

2 Degaussing

A degaussing procedure is necessary to magnetize the mumetal layers. This procedure is necessary to ensure the best shielding factor and therefore as small a residual field inside the cube as possible. To that purpose, ideally the external field conditions are constant in time and identical to the conditions in which the mumetal shielding is to perform. The magnetization within the mumetal then is achieved by means of degaussing coils placed along the sides of the cube. They produce a field degaussing each spatial axis separately, the order of degaussing being of no consequence to the magnetization [5]. Figure **??** shows the degaussing coils inside the mumetal cube inside white strips along the cube edges.

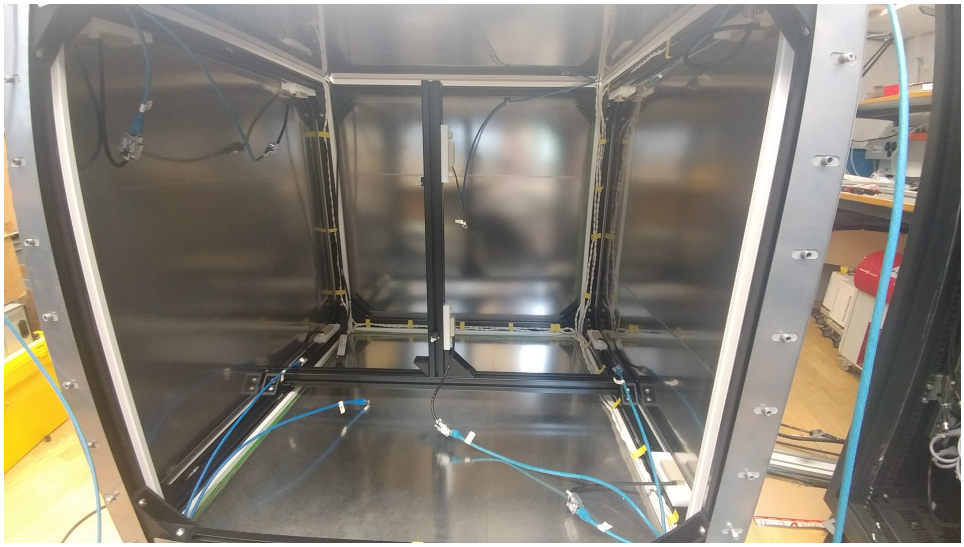

Figure 1: Inside the mumetal cube. Degaussing coils are seen in white along the edges. Fluxgate magnetometers are present as well and have blue CAT5 cables attached.

In order to degauss the mumetal, for each spatial axis successively, a sinusoidal current of initially exponentially decreasing amplitude and 10 Hz frequency is put through the coils. Below a set threshold, the amplitude is set to decrease linearly to zero. The entire procedure takes 60 s per spatial axis.

More precisely, the degaussing coils are installed in an L-shaped pattern, covering two spatial axes per coil. The degaussing procedure therefore covers a plane spanned by two axes per succession.

The signal is produced by a Raspberry Pi computer with a built-in 16 bit DAC, connected to an amplifier that creates the current needed for the coils. Prior to the degaussing procedure, the offset is set to zero at the amplifier such that residual currents remain below 1×10^{-4} A when the Raspberry Pi is actively sending an signal of zero amplitude.

In order to properly magnetize the mumetal shielding, it has to be driven into saturation by the degaussing coils with the initial peaks of the signal. A pickup coil follows the wiring of the degaussing coils. To ascertain whether the mumetal is driven into saturation by the current coils, a 2D hysteresis curve is plotted on the oscilloscope with the sinusoidal signal as the y-axis and the voltage from the pickup coil as the x-axis. The obtained curve can be see in image 2.

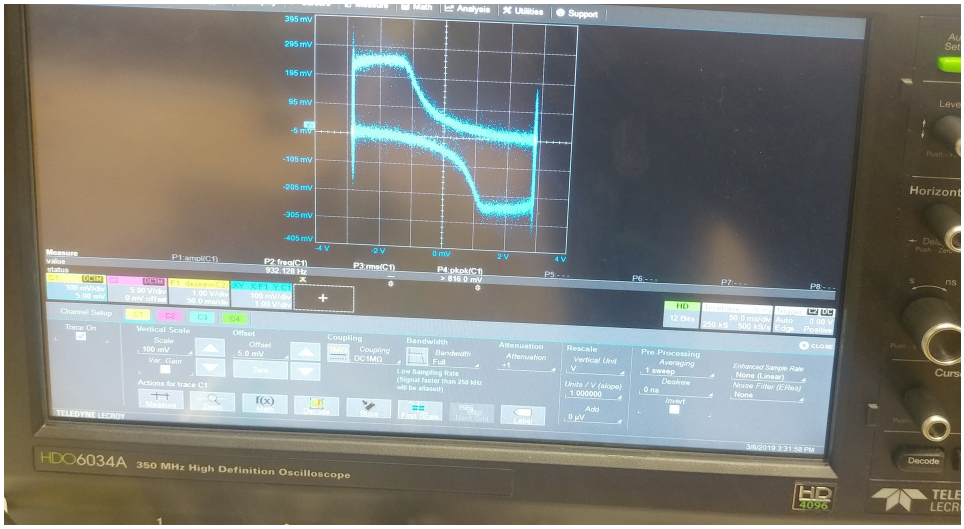

Figure 2: Hysteresis curve obtained with the sinusoidal signal from the Raspberry Pi as y-axis and pickup coil voltage as x-axis at maximal sinusoidal amplitude.

The abrupt cut in the x-axis shows that the pickup coil does not generate voltages greater in amplitude than roughly 3 V. This is due to the mumetal being driven to saturation at peak signal amplitudes and thus not delivering higher magnetic fields than observed by the pickup coil.

3 Setup

For the generation of external magnetic fields, a surrounding field compensation (SFC) apparatus is employed. The SFC consists of a system of coils with an intricate geometry allowing for the creation of highly homogeneous magnetic fields [6]. The mumetal cube is placed in the SFC with 8 external and 10 internal fluxgates of type $FLC3-70$ [7] as magnetometers. All fluxgates are mounted onto non magnetic plastic profiles to avoid them coupling to a magnetic surface, thus locally changing the magnetic field. Figure 3 shows the mumetal cube situated within the SFC structure.

Figure 3: Mumetal cube inside the SFC structure.

The external fluxgates are mounted on the same positions as the internal ones with respect to both the x and z axes. Figure 4 shows the fluxgates within the setup. Additionally, figure 5 illustrates the geometric placements and distances between the fluxgates.

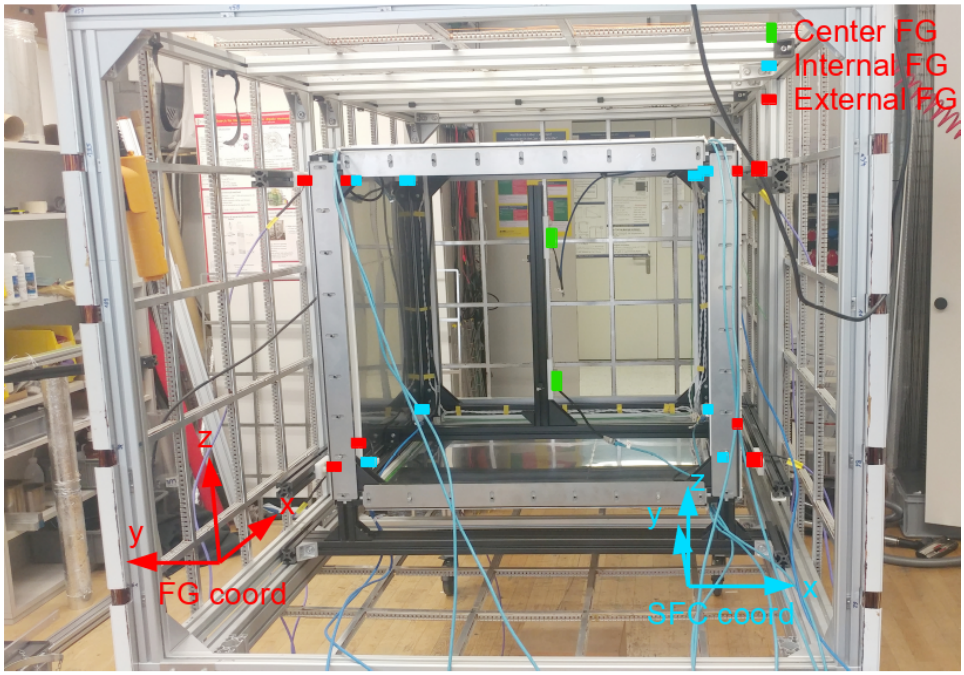

Figure 4: Mumetal cube with two sides missing in SFC structure with external fluxgates (red), internal and central fluxgates (blue and green respectively). SFC coordinates are shown in blue, fluxgate, ie. system coordinates in red.

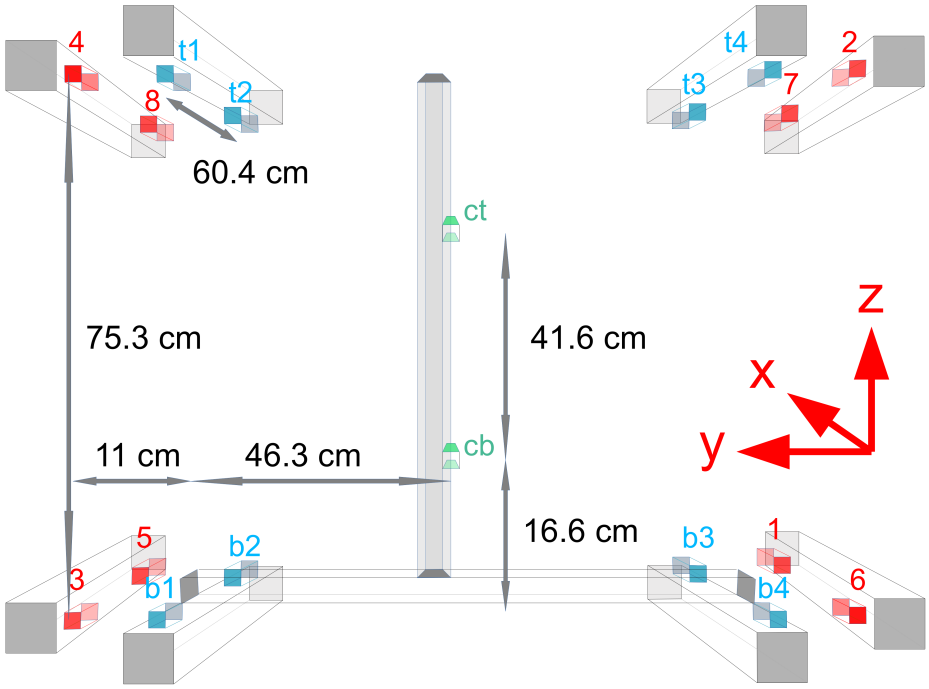

Figure 5: Schematic of fluxgates with distances and labels. In tones of grey, the item profiles onto which the fluxgates are mounted are shown. Red are the outer fluxgates, blue the ones within the mumetal and in green the central fluxgates. The system coordinates are represented with thick red arrows. The red and blue fluxgates pairwise share coordinates except in the y direction. For example, fluxgates 3 and $b1$ have identical x and z coordinates, the same holds true for 5 and $b2$ and so on. The green fluxgates are centered the x-y plane. The shown distances are center-to-center distances between fluxgates.

The fluxgate data is recorded by means of a *National Instruments* $PXI-1033$ DAQ system [8]. All data is taken at 1 kHz sampling rate and $\pm$ 10 V range with 18 bit resolution.

Measurements are taken with several configurations of the mumetal cube, the SFC remaining in a fixed position. Initially, background measurements are taken during a period of 180 s with only fluxgates 1-8 mounted on the SFC structure, see figure 5. During the background measurement, the cube is taken outside the room and remains located several meters from the SFC to minimize its interference with background fields. Additionally, we

measure with the full cube inside the SFC, as well as the cube with two sides removed with all fluxgates, except one. Fluxgate $t4$ is omitted as the DAQ system did not support the number of channels necessary for all fluxgate data. Upon removing two opposing faces, the cube is subjected to a further degaussing procedure to account for the new geometry of shielding material. Due to the missing faces along one axis, only the single pair of coordinate axes perpendicular to it manifests a hysteresis curve like the one in figure 2.

Some fluxgates were found to saturate due to fields outside their range. This effect manifests through clipping when the fluxgates measure fields greater in amplitude than 155 μT, see figure 6. A threshold is set at 150 μT and datapoints exhibiting greater fields are omitted from the analysis.

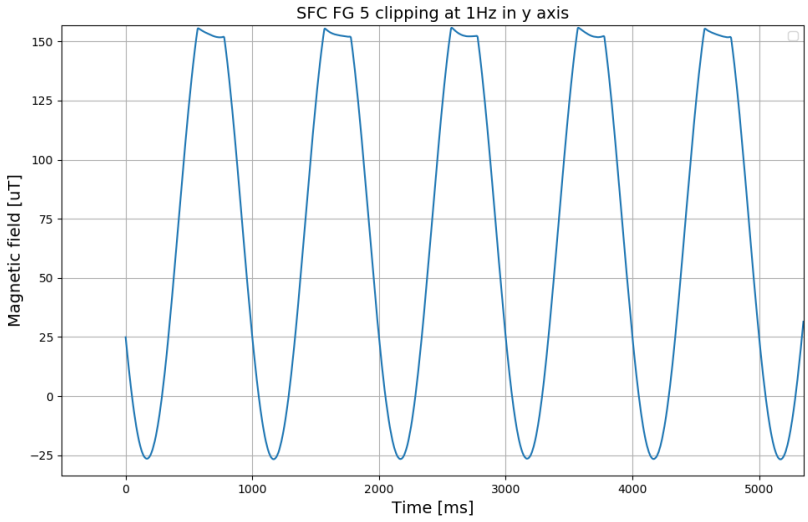

Figure 6: Clipping observed by fluxgate 5 at 1 Hz along the y axis with full cube setup.

4 Shielding factor

In an ideal situation, to measure the shielding factor, fluxgate magnetometers should be placed in identical locations with and without mumetal. However, the bulk of the measurements was taken with only the SFC fluxgates mounted, assuming a sufficiently high homogeneity of the magnetic fields produced therein. In an additional set of measurements, the two central

fluxgates were placed at the same locations they would sit within the cube, but without the latter. In this setup, only the frequencies DC, .1 Hz, .5 Hz, 1 Hz, 2 Hz, 5 Hz were applied and measured with. To determine the shielding factor $F_{shielding}$, the peak-to-peak values of the magnetic field observed by the fluxgates Vpp is taken for the case with and without mumetal and the absolute value of ratio of the two is taken:

$$F_{shielding} = \left| \frac{Vpp_{\text{no mumetal}}}{Vpp_{\text{mumetal}}} \right| \tag{1}$$

Figure 7 shows the shielding factor obtained with the full cube from the data measured with the top center fluxgate (ct), figure 8 the same for the center bottom (cb) fluxgate. Figure 9 shows the same results for the situation in which the cube is missing two opposing faces, while figure 10 shows the latter from the center bottom fluxgate (cb) perspective. Figure 11 shows the shielding factor obtained for the gradient along the z axis.

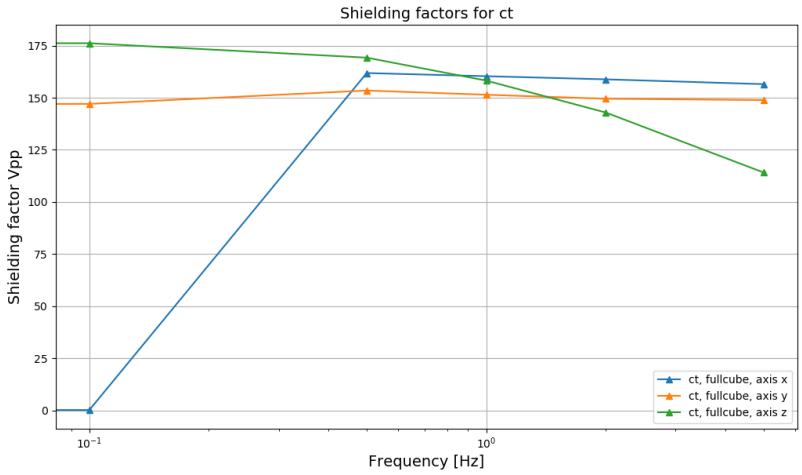

Figure 7: Shielding factor obtained with full cube for all three axes with center top fluxgate (ct).

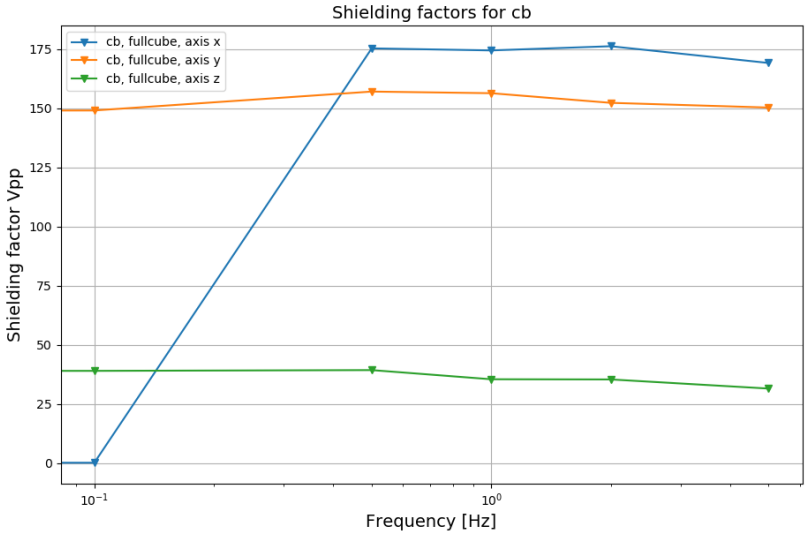

Figure 8: Shielding factor obtained with full cube for all three axes with center top fluxgate (ct).

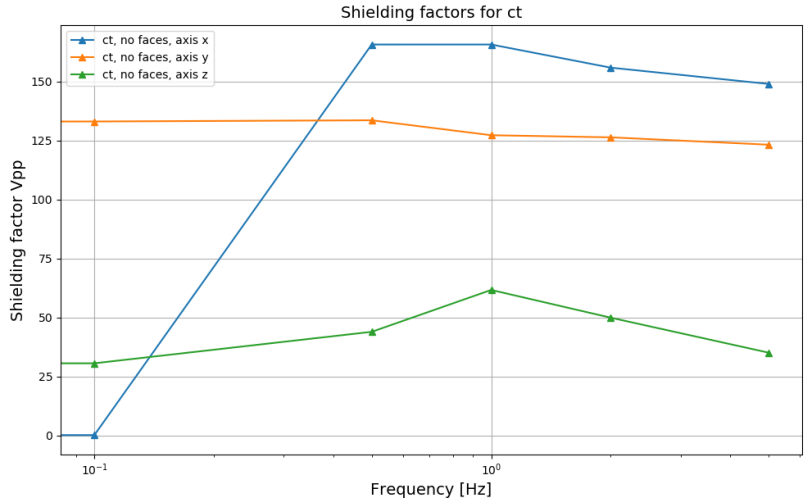

Figure 9: Shielding factor obtained with cube missing two faces for all three axes with center top fluxgate (ct).

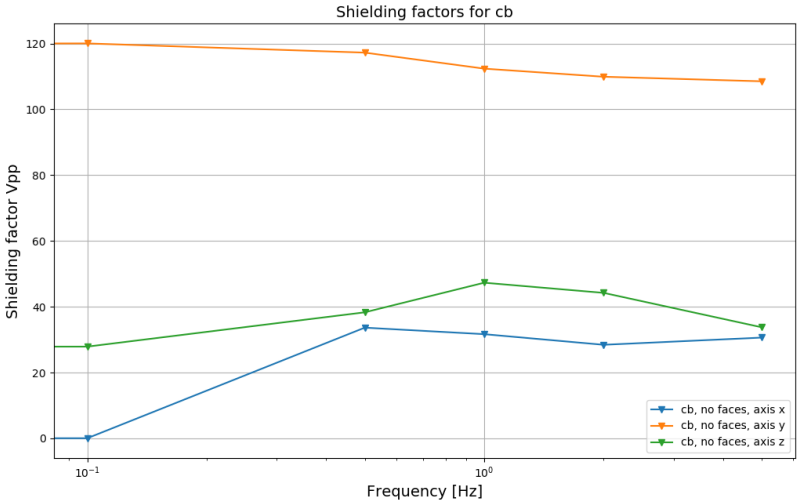

Figure 10: Shielding factor obtained with cube missing two faces for all three axes with center bottom fluxgate (cb).

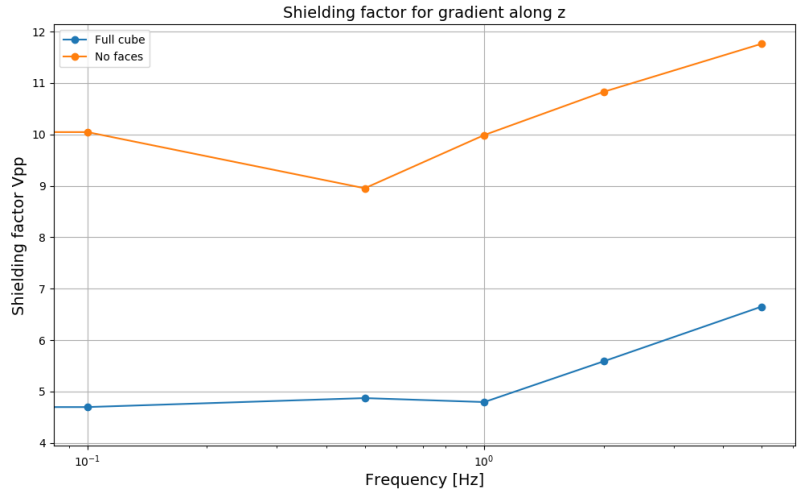

Figure 11: Shielding factor for the gradient field along z axis.

To illustrate the method of peak-to-peak amplitudes employed, figure 12 shows the data as observed by fluxgatte *cb* for a DC measurement for both

the situation with a full mumetal cube and no mumetal. A modulation of the magnetic field is observed with an amplitude of roughly 12 μT for the case without mumetal. To examine this, the signal is subjected to a discrete Fourier transform, see figure 13 for the plot. The biggest peak is observed at 50 Hz, stemming in all likelihood from the electrical sockets in the room.

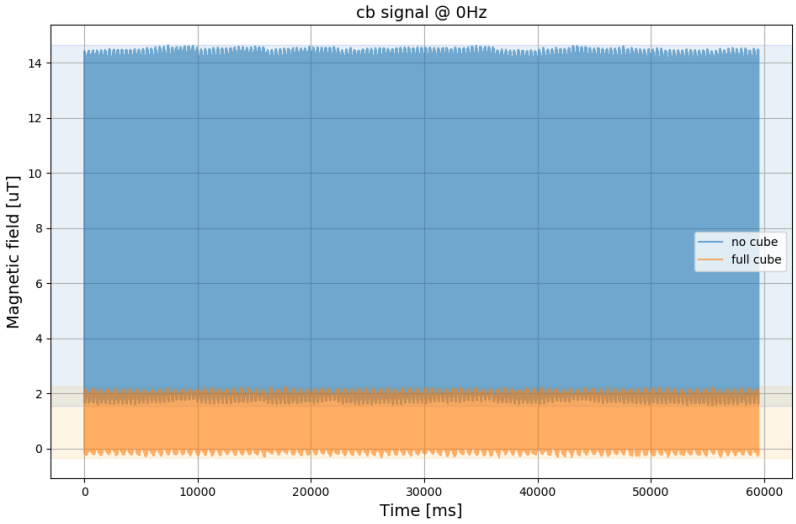

Figure 12: DC data with no mumetal and full cube.

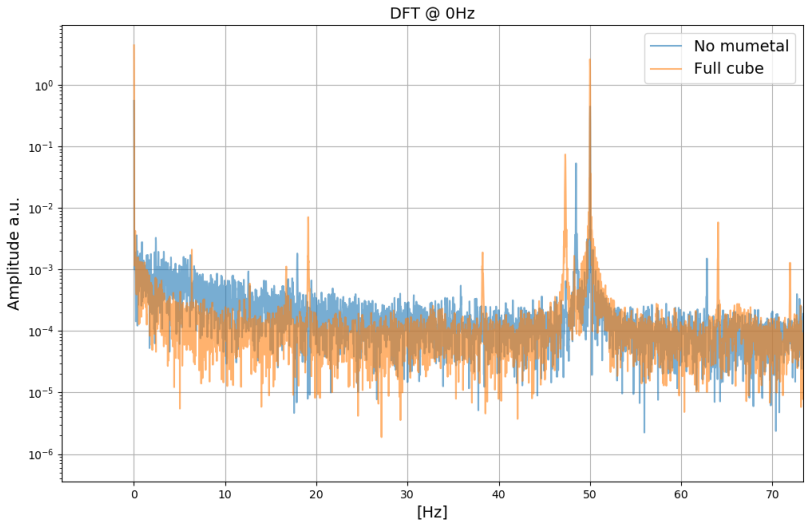

Figure 13: Discrete Fourier transform of *cb* axis z with no mumetal and full cube at 0 Hz, zoomed to reveal the spectrum from 0 Hz to 70 Hz.

Furthermore, the shielding factor is considered for all fluxgates except the central ones. To this end, the close proximity of fluxgate pairs such as (3,$b1$) is used to approximate their position, assuming also a sufficiently homogeneous field between their respective positions, as identical. Hence, the shielding factor is computed following equation 2 by taking the closest fluxgate pairs with and without mumetal, namely the pairs (3,$b1$), (5,$b2$), (1,$b3$), (6,$b4$), and similarly, for the upper fluxgates: (4,$t1$), (8,$t2$), (7,$t3$). The measurements were taken by applying a magnetic field of frequencies DC, .1 Hz, .5 Hz, 1 Hz, 2 Hz, 5 Hz, 10 Hz, 20 Hz, 40 Hz, 60 Hz, 100 Hz. Figures 14-16 show the shielding factors so obtained as a function of frequency for the full mumetal cube, figures 17-19 in turn for the setup where two faces of the cube are removed.

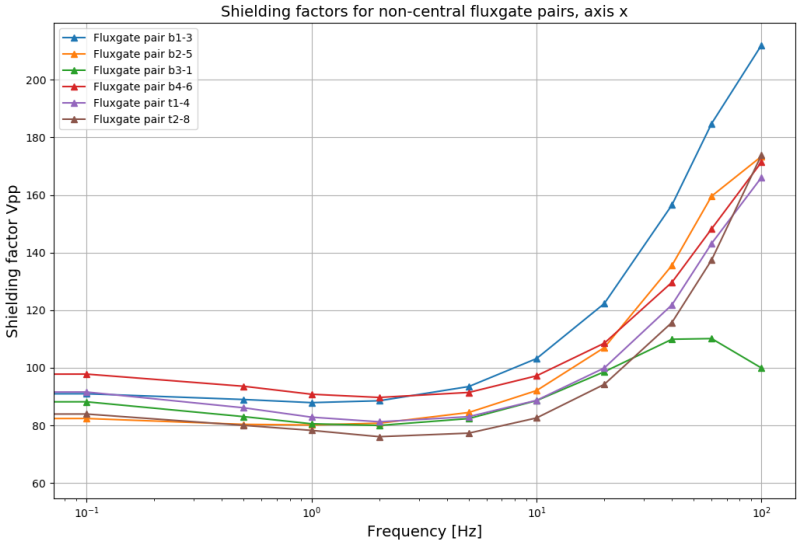

Figure 14: Shielding factor along the x axis of non-central fluxgate pairs as a function of frequency of applied fields for the full mumetal cube configuration. The pair involving fluxgate $t3$ is omitted due to unphysical behaviour.

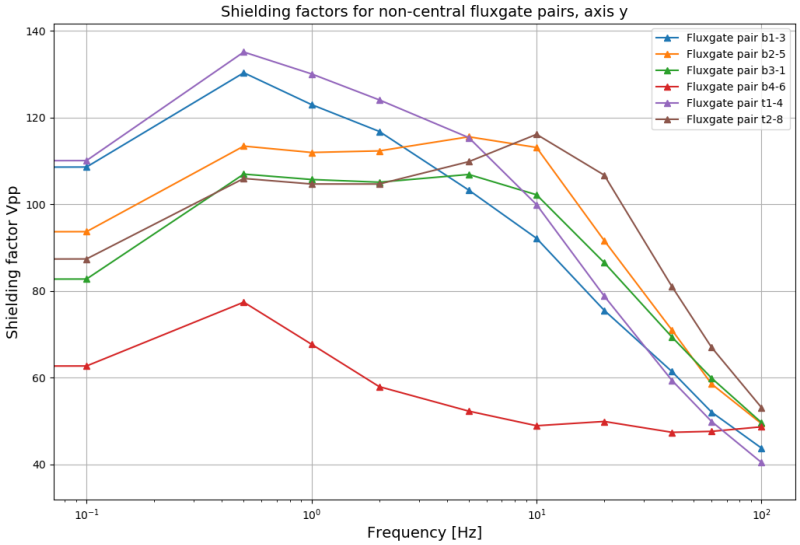

Figure 15: Shielding factor along the y axis of non-central fluxgate pairs as a function of frequency of applied fields for the full mumetal cube configuration. The pair involving fluxgate $t3$ is omitted due to unphysical behaviour.

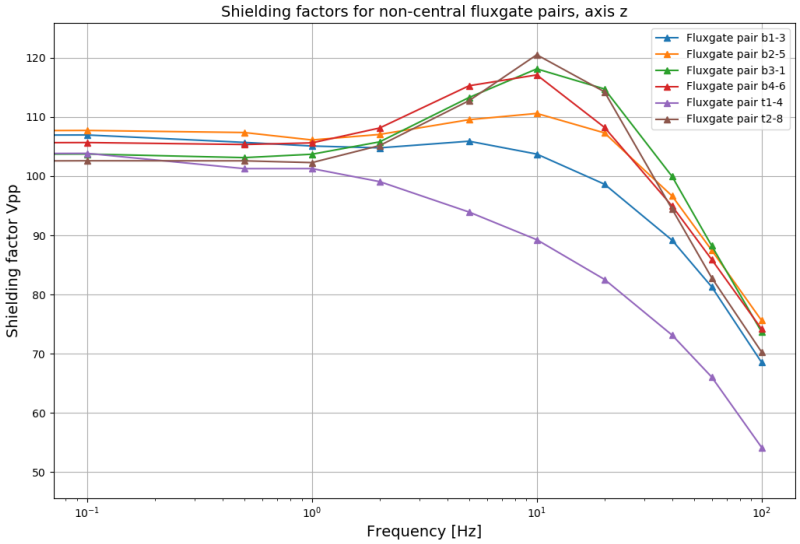

Figure 16: Shielding factor along the z axis of non-central fluxgate pairs as a function of frequency of applied fields for the full mumetal cube configuration. The pair involving fluxgate $t3$ is omitted due to unphysical behaviour.

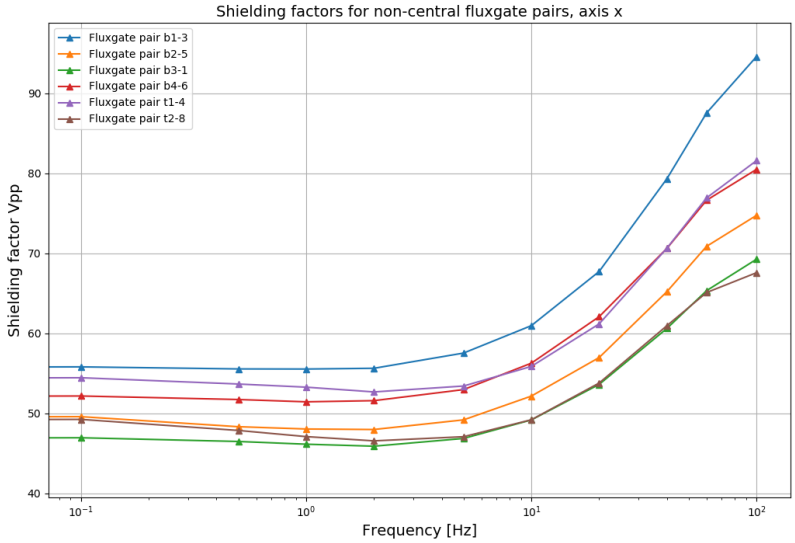

Figure 17: Shielding factor along the x axis of non-central fluxgate pairs as a function of frequency of applied fields for the mumetal cube missing two faces configuration. The pair involving fluxgate $t3$ is omitted due to unphysical behaviour.

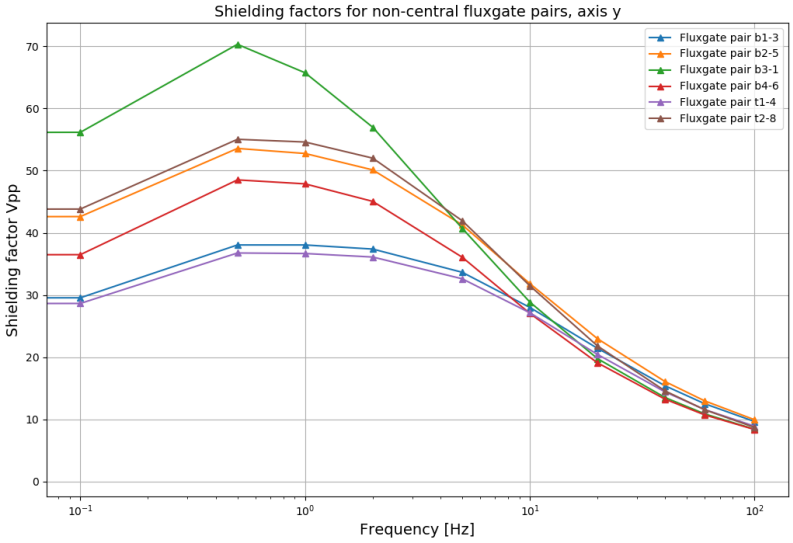

Figure 18: Shielding factor along the y axis of non-central fluxgate pairs as a function of frequency of applied fields for the mumetal cube missing two faces configuration. The pair involving fluxgate $t3$ is omitted due to unphysical behaviour.

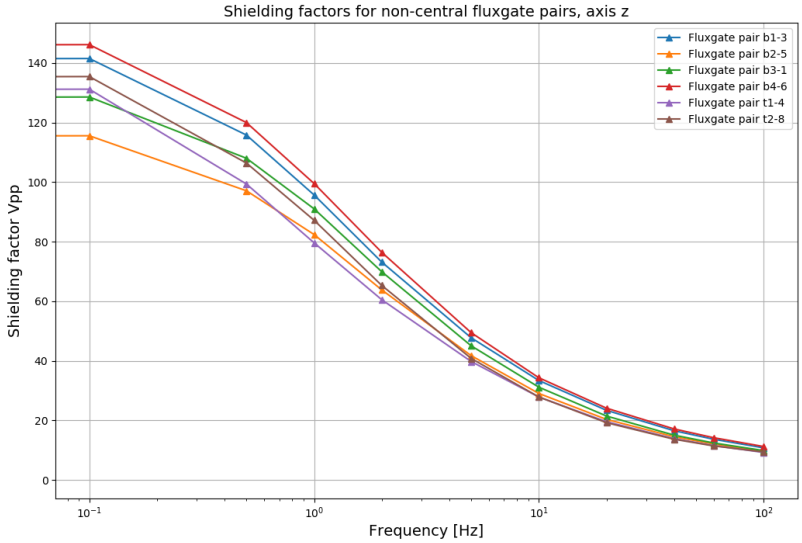

Figure 19: Shielding factor along the z axis of non-central fluxgate pairs as a function of frequency of applied fields for the mumetal cube missing two faces configuration. The pair involving fluxgate $t3$ is omitted due to unphysical behaviour.

As a general remark, the shielding factor, as expected, appears to decrease with increasing frequency of the applied fields. This trend however is reversed for the cube with missing faces along the axis of the latter, indicating that the magnetic flux is more efficiently guided around the mumetal cube at higher frequencies in this setup.

On the other hand, the shielding capability of the cube without two faces along the z axis, the axis of interest for the beam EDM experiment, drops much more quickly as the frequency of external fields increase than is the case for the full cube.

5 Homogeneity

To examine the homogeneity of the magnetic field within the SFC, a complete three dimensional map would be necessary. In order to examine the homogeneity with the available data however, a reference fluxgate is chosen. Subsequently and for each spatial axis, the absolute difference of the mean magnetic field observed by all ordered pairs of fluxgates is constructed as a

function of the frequency of the applied field the distance along the chosen axis between pair of fluxgates. This is shown in equation 2, with ref as reference, FGi designating the i-the fluxgate in the pairs, and $R_i(freq)$ the corresponding field change per centimeter. For the case without mumetal, *cb* is chosen for reference and the corresponding field changes are plotted in figures 20-22.

$$R_i(freq) = \left| \frac{\bar{B}_{\mathrm{FGref}}(freq) - \bar{B}_{\mathrm{FGi}}(freq)}{\Delta x} \right| \tag{2}$$

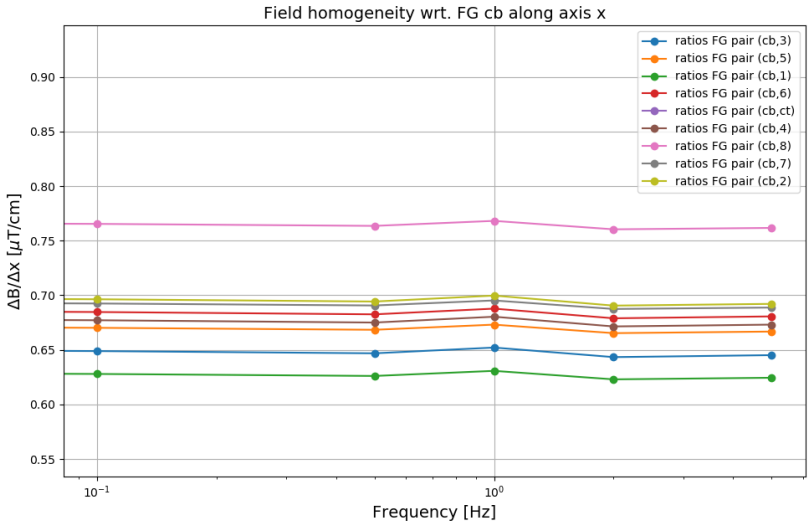

Figure 20: Pairwise changes of mean magnetic fields per centimeter as a function of frequency of applied field, axis x.

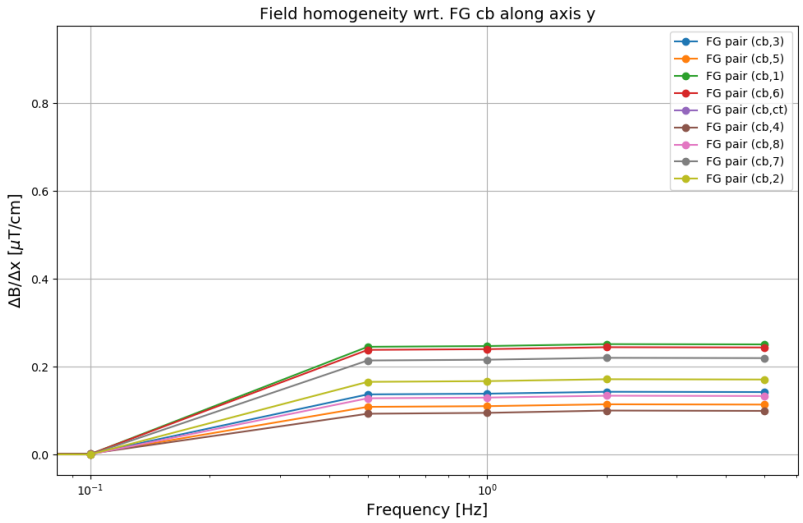

Figure 21: Pairwise changes of mean magnetic fields per centimeter as a function of frequency of applied field, axis y.

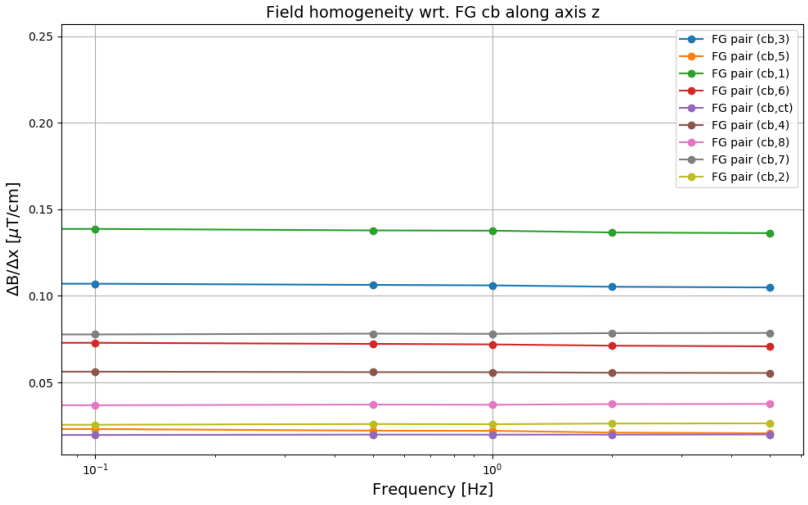

Figure 22: Pairwise changes of mean magnetic fields per centimeter as a function of frequency of applied field, axis z.

Since the SFC is built such that one face of the coil holding structure is missing along the x-axis, the highest inhomogeneities are expected, and indeed observed along the latter. The z axis, which is also the axis of quantization in the future Beam EDM experiment, exhibits the highest homogeneity, not exceeding the value of 0.14 $\mu T/cm$.

6 Conclusion

It is unclear, whether the degaussing order plays a role for the case of broken symmetry whence two faces of the mumetal cube are missing. Further experimental analysis of this case would benefit a complete picture of the shielding behaviour.

A more complete magnetic field map would be highly beneficial to reconstruct and correct for the background fields in the room, as well as to ascertain the SFC properties in the magnetic fields. A further study thereof and combination of new data would help to further the present analysis.

A different definition of the shielding factor, taking not only peak-to-peak oscillations of the magnetic fields, but also the shift of the mean value of magnetic fields into account could give a more detailed picture of the shielding capabilities of the mumetal construction.

References

[1] E. Chanel, Z. Hodge, D. Ries, I. Schulthess, M. Solar, T. Soldner, O. Stalder, J. Thorne, and F. M. Piegsa. The pulsed neutron beam edm experiment. *arXiv:1812.03987*, 2018.

[2] J. M. Pendlebury, S. Afach, N. J. Ayres, C. A. Baker, G. Ban, G. Bison, K. Bodek, M. Burghoff, P. Geltenbort, K. Green, W. C. Griffith, M. van der Grinten, Z. D. Grujić, P. G. Harris, V. Hélaine, P. Iaydjiev, S. N. Ivanov, M. Kasprzak, Y. Kermaidic, K. Kirch, H.-C. Koch, S. Komposch, A. Kozela, J. Krempel, B. Lauss, T. Lefort, Y. Lemière, D. J. R. May, M. Musgrave, O. Naviliat-Cuncic, F. M. Piegsa, G. Pignol, P. N. Prashanth, G. Quéméner, M. Rawlik, D. Rebreyend, J. D. Richardson, D. Ries, S. Roccia, D. Rozpedzik, A. Schnabel, P. Schmidt-Wellenburg, N. Severijns, D. Shiers, J. A. Thorne, A. Weis, O. J. Winston, E. Wursten, J. Zejma, and G. Zsigmond. Revised experimental upper limit on the electric dipole moment of the neutron. *Phys. Rev. D*, 92:092003, Nov 2015.

[3] Norman F. Ramsey. A molecular beam resonance method with separated oscillating fields. *Phys. Rev.*, 78:695–699, Jun 1950.

[4] C. P. Bidinosti and J. W. Martin. Passive magnetic shielding in static gradient fields. *AIP Advances*, 4(4):047135, 2014.

[5] Igor Altarev, Earl Babcock, D Beck, M Burghoff, S Chesnevskaya, T Chupp, S Degenkolb, I Fan, P Fierlinger, A Frei, Erwin Gutsmiedl, S Knappe-Grüneberg, Florian Kuchler, Thorsten Lauer, Peter Link, T Lins, Michael Marino, J McAndrew, B Niessen, and T Zechlau. A magnetically shielded room with ultra low residual field and gradient. *The Review of scientific instruments*, 85, 03 2014.

[6] Beatrice Franke. *Investigations of the internal and external magnetic fields of the neutron electric dipole moment experiment at the Paul Scherrer Institute*. PhD thesis, ETH Zurich, 2013. Diss., Eidgenössische Technische Hochschule ETH Zürich, Nr. 21562, 2013.

[7] Magnetic field sensor flc3-70.

[8] *NI PXI-1033 User Manual*.